IEEE Access
Multidisciplinary | Rapid Review | Open Access Journal

Received May 11, 2020, accepted May 21, 2020, date of publication May 25, 2020, date of current version June 8, 2020.

Digital Object Identifier 10.1109/ACCESS.2020.2997517

SM-PI Control Strategy of Electric Motor-Pump for Pure Electric Construction Machinery

SHENGJIE FU, HAOLING REN, TIANLIANG LIN, SHENGYAN ZHOU, QIHUAI CHEN, (Member, IEEE), AND ZHONGSHEN LI

College of Mechanical Engineering and Automation, Huaqiao University, Xiamen 361021, China

Corresponding author: Tianliang Lin (ltlkxl@163.com)

This work was supported in part by the National Natural Science Foundation of China under Grant 51875218 and Grant 51905180, in part by the Excellent Outstanding Youth Foundation of Fujian Province of China under Grant 2018J06014, in part by the Industry Cooperation of Major Science and Technology Project under Grant 2019H6015, in part by the Natural Science Foundation of Fujian Province under Grant 2018J01068 and Grant 2019J01060, and in part by Hitachi Construction Machinery Company Ltd.

ABSTRACT Although the pure electric drive system is widely applied to mobile machines, it is not easy for construction machinery (CM) to realize electrification because of the different working style. The CM load changes dramatically and continuously, and the traditional PI control cannot handle this condition. A vector control strategy based on speed sliding mode control (SMC) and torque PI control is proposed for CM with the characteristic of drastically changing loads. Based on the mathematical model of an electric motor-pump, the electric motor-pump control performance requirement for electric CM is analyzed. Combined with the permanent magnet synchronous motor (PMSM) mathematical model, the speed SMC-PI observer is designed. The controller is designed using an exponential approximation method and uses integral and differential links, which has excellent robustness, to suppress flutter in SMC-PI. Control strategies of speed loops with PI and SMC-PI were compared under different conditions. The overshoot of the motor-pump speed was small and zero static control could be achieved. When the load was variable, the fluctuation of rotation speed was approximately 0.5% $\sim$ 1% with SMC-PI, which is only 25% $\sim$ 50% of PI control. Finally, the vector control algorithm based on speed SMC-PI was tested on a hydraulic excavator driven by the electric motor. The test results show that the vector control base on speed SMC-PI achieved a maximum static difference of rotational speed of approximately 1%. When the load power was close to 50% of the rated power, the electric motor-pump speed fluctuation range was -5% $\sim$ 5%, and the steady-state error was only approximately 0.3%.

INDEX TERMS Construction machinery, sliding mode control, PI control, electric drive, energy saving, electric motor.

I. INTRODUCTION

Nonroad moving machinery (NRMM), represented by construction machinery (CM) with internal combustion engines (ICE) as the main driving power, emits 909,000 tons of sulfur dioxide and 5.735 million tons of nitrogen oxides. With increasingly strict emission requirements, electric CM has become the focus of the development. Electric CM adopts an electric motor instead of a traditional ICE, which can achieve the purpose of low noise and zero emission. With the electric motor as the power source, the braking energy generated during the braking process can be electrically recovered and stored to further improve energy utilization. At present, the electric motor-pump and its control technology for electric vehicles are relatively mature, but due to the complexity and variability of CM load characteristics, the frequency converter used in the industrial field and the electric motor controller for electric vehicles cannot be directly transmitted to CM. Due to the CM load characteristics, research on electric motor-pump control technology has gradually attracted attention. Wang *et al.* adopted the current loop and speed loop of the permanent magnet motor control system to control and compensate for the potential energy of CM arms, which improved the anti-interference capability of the system [1]. Chen *et al.* designed a power motor according to the working characteristics of hybrid CM, and tested the motor control method by adopting the vector control. The results showed that the dynamic characteristics of the power system and the

The associate editor coordinating the review of this manuscript and approving it for publication was Huanqing Wang.

energy savings of the system were improved [2]. Han *et al.* employed a motor to replace the hydraulic motor of the hybrid excavator. The motor was controlled by vector control and a supercapacitor was used to recover the electric energy. The proposed scheme can reduce the energy consumption of CM during the swing process [3]. Lin *et al.* adopted the method of direct torque control to avoid current shock and mutation through torque limitation and realized flexible control of electricity-driven CM at the expense of response and control voltage [4]. Chang *et al.* proposed a nonfragile H ∞ filter design to control the motor system which can effectively reduce the disturbance noise [5]. Yao adopted an active disturbance rejection adaptive controller to improve tracking performance and the test results showed that the proposed control strategy can achieve high tracking performance [6]. At present, relevant studies on electric motor control for CM are mostly used for rotary conditions or auxiliary driving, while the studies on electric motor control strategies directly based on load characteristics of CM are few.

The mainly used electric motor control strategies are vector control and direct torque control (DTC). Due to the large torque ripple and poor low-speed performance, DTC has a relatively small application range [7]. Vector control adopts the method of coordinate transformation to decouple the mathematical model of an AC motor, which can be controlled by an equivalent AC to DC motor [8]. In addition, the performance of speed regulation is greatly improved. The traditional vector control adopts the closed-loop control method of rotational speed and current PI. PI control has the advantages of simple structure and easy implementation, but it has the disadvantages of poor robustness and poor anti-interference ability [9]–[12] and cannot well adapt to the characteristics of CM. The parameter setting of the traditional PI control needs to balance the dynamic response and system stability, which cannot be balanced well and can result in poor control performance when the load changes dramatically and continuously. Although there are relatively advanced particle swarm optimization algorithms that can adjust and optimize PI control, they are not suitable for CM whose condition is complex and changeable [13], [14].

Sliding mode control (SMC) is a nonlinear control method [15], [16]. The design of sliding mode is independent of system parameters and external interference and has good robustness and anti-interference capability [17]. Scholars have also carried out relevant studies on the application of SMC in the field of electric motor control, realizing the estimation and adjustment of flux, current and speed [18]–[20]. Wang *et al.* established a tracking control system of an adaptive fuzzy sliding mode by incorporating the integral term of the output tracking error. Under the unknown disturbances, accessibility can still be ensured by the proposed tracking control. In addition, the proposed adaptive fuzzy sliding mode controller is demonstrated to be feasible and superior [21], [22].

Considering the complexity and variability of load characteristics of CM, a vector control strategy based on speed SMC and torque PI control, which is called SMC-PI in this paper, is proposed to improve the robustness of electric motor-pump speed and suppress speed fluctuation caused by drastic changes of the external load. Then, the electric CM performance can be improved. The article is organized as follows. The mathematical model analysis of electric motor-pump and PMSM is presented in the "MATHEMATICAL MODEL ANALYSIS" section. The design of the electric motor-pump control strategy and regulators is presented in the "ELECTRIC MOTOR-PUMP CONTROL STRATEGY RESEARCH" section. The experiments under different conditions are shown in the "EXPERIMENTAL STUDY" section. Concluding remarks are given in the "CONCLUSION".

II. MATHEMATICAL MODEL ANALYSIS

To better adapt the motor control strategy to the load characteristics of CM, an analysis of the mathematical model of the system power unit is used to design the electric motor-pump control strategy. Through the analysis of the mathematical model of a hydraulic pump, the influence of electric motor-pump control performance on the hydraulic system is studied. The requirement of the electric motor-pump control used in the hydraulic system is proposed. Accordingly, the electric motor-pump regulator is designed combined with the mathematical model.

A. MATHEMATICAL MODEL ANALYSIS OF ELECTRIC MOTOR-PUMP

As the power unit of hydraulic systems, the working state of the hydraulic pump directly affects the maneuverability and stability of CM. Therefore, from the mathematical model of the hydraulic pump, the influence of the electric motor-pump control system on the working characteristics of the hydraulic pump is analyzed, and then the requirements for an electric motor-pump control system are proposed. For convenience, the schematic diagram of the hydraulic system is simplified in Fig. 1 to analyze the characteristics of the hydraulic pump.

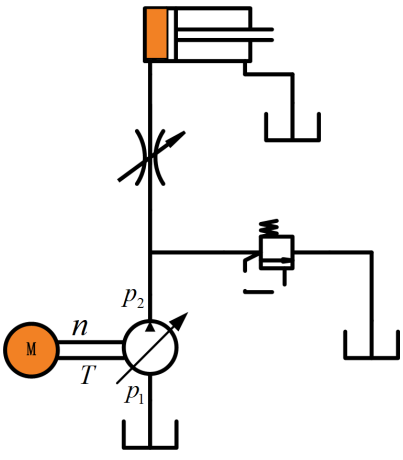

FIGURE 1. Simplified schematic of hydraulic system.

The oil is supplied to the actuator through the pump driven by the electric motor, and the safe pressure of the system is regulated by the relief valve. The symbols used are defined as follows: the electric motor-pump speed is n, the torque is T, the inlet pressure of the pump is p_1, the outlet pressure is p_2, and the displacement of the pump is V.

In the hydraulic system shown in Fig. 1, the flow continuity equation of the pump is

$$\begin{aligned} Q_1 &= nV - k_1\Delta p - k_2\sqrt{\Delta p} + C_1\frac{dp_1}{dt} \\ Q_2 &= nV - k_1\Delta p - k_2\sqrt{\Delta p} + C_2\frac{dp_2}{dt} \end{aligned} \tag{1}$$

where Q_1 and Q_2 are the flow rate into and out of the pump, respectively; Δp is the pressure differential; C_1 and C_2 are the liquid capacitance of the absorption and discharging cavity, respectively; k_1 and k_2 are the coefficient of the laminar and turbulent of the pump, respectively.

During the dynamic adjustment of the hydraulic pump, the liquid capacity of the hydraulic pump can be neglected compared with the pipeline cavity and the accumulator. Then, equation (1) can be simplified to

$$Q = nV - \Delta\text{Q-C}\frac{d\,\Delta p}{dt} \tag{2}$$

where ΔQ is the inner leakage of the pump.

The balance equation of the internal discharge force of the hydraulic pump is

$$p_2 = R\Delta Q + L\frac{d\,\Delta p}{dt} \tag{3}$$

where R and L are equivalent liquid resistance and liquid inductance of the system, respectively. In the constant displacement system, the liquid inductance can be further expressed as

$$L = \frac{\Delta p}{Vdn/dt} \tag{4}$$

Apply Laplace transform to equations (2) and (3) to obtain the transfer function of pressure and flow of the pump outlet.

$$G(s) = \frac{P_2(s)}{Q(s)} = -\frac{R(L/R\cdot s+1)}{LCs^2 + RCs + 1} \tag{5}$$

It can be seen from equation (5) that the transfer function of pressure and the flow of the pump outlet is a second-order system, and the natural frequency and damping ratio of the system are

$$\begin{cases} \omega = \sqrt{\dfrac{1}{LC}} \\ \xi = \dfrac{R}{2}\sqrt{\dfrac{C}{L}} \end{cases} \tag{6}$$

The torque equation of the hydraulic pump is

$$T_p = T_c + b_0 n + b_1 n^2 + (\frac{V}{2\pi} + k_3)\Delta p \tag{7}$$

where T_c is the torque loss independent of speed, b_0 is the viscous damping coefficient, b_1 is the torque loss coefficient caused by fluid flow and turbulence leakage, and k_3 is the torque loss coefficient of the sealing surface caused by pressure loss.

In the constant displacement system, if the pressure differential between the inlet and outlet of the pump remains unchanged, the output torque of the pump will be minimized when the pump speed $n = b_0/(2\ b_1)$. Minimizing the torque of the pump is

$$T_{\min} = T_{\text{cp}} - \frac{b_0^2}{4b_1} \tag{8}$$

To reduce the influence of the inner leakage of the hydraulic pump on the pump outlet pressure, methods such as increasing the elastic modulus of the hydraulic oil, reducing the volume of the cavity and fluid inductance can be adopted. Combined with equations (4) and (6), it can be seen that the faster the electric motor-pump speed response is, the smaller the liquid inductance, and the larger the natural frequency is, the more obvious the suppression effect of internal leakage. At the same time, the fluctuation in electric motor-pump speed will lead to the fluctuation of hydraulic pump torque, which will directly affect the control and stability of the system. The response speed of a permanent magnet synchronous motor (PMSM) is much faster than that of a hydraulic pump. Therefore, the influence of speed fluctuation on the system should be given priority when controlling the electric motor-pump. In addition, the target is to improve the robustness and anti-interference ability of speed.

B. MATHEMATICAL MODEL ANALYSIS OF PMSM

The operational efficiency of PMSM is up to 97% [20], and it has the advantages of excellent speed regulation performance, high operational efficiency, high power density, small size and easy maintenance. PMSM is widely used in electric vehicles [24]–[26]. Since an AC motor is a high-order, nonlinear, multivariable and strongly coupled system, vector coordinate transformation is usually used to decouple the mathematical model of the electric motor into a two-phase rotating coordinate system.

According to the principle that the magnet motive force and the power remain unchanged before and after the coordinate transformation, vector coordinate transformation is carried out for the PMSM mathematical model. The PMSM mathematical model can be decomposed into a two-phase rotating coordinate system by Clark and Park transformation. The electric motor voltage equation in the two-phase rotating coordinate system is

$$\begin{cases} u_{\text{d}} = \dfrac{d\psi_{\text{d}}}{dt} - \omega\psi_{\text{q}} + R_{\text{s}}i_{\text{d}} \\ u_{\text{q}} = \dfrac{d\psi_{\text{q}}}{dt} + \omega\psi_{\text{d}} + R_{\text{s}}i_{\text{q}} \end{cases} \tag{9}$$

where subscripts d and q are the components of the d and q axes, respectively in the rotating coordinate system; u is the stator flux linkage of stator voltage Ψ; ω is the angular velocity; R_{s} is stator resistance of the electric motor.

The flux linkage equation is

$$\begin{cases} \psi_{\mathrm{d}} = L_{\mathrm{d}} i_{\mathrm{d}} + \psi_{\mathrm{f}} \\ \psi_{\mathrm{q}} = L_{\mathrm{q}} i_{\mathrm{q}} \end{cases} \tag{10}$$

where L_{d} and L_{q} are the inductive component of the d and q axes, respectively.

The torque equation is

$$T_{\mathrm{e}} = p\left[\psi_{\mathrm{f}} i_{\mathrm{q}} + (L_{\mathrm{d}} - L_{\mathrm{q}})_{\mathrm{q}} i_{\mathrm{d}} i_{\mathrm{q}}\right] \tag{11}$$

If the tab-stick PMSM is adopted, the inductances of the quadrature and straight shafts of the electric motor are approximately equal, and equation (11) can be expressed as

$$T_{\mathrm{e}} = p\psi_{\mathrm{f}} i_{\mathrm{q}} \tag{12}$$

It can be seen from equation (12) that in the two-phase rotating coordinate system, the mathematical model of the electric motor is decoupled. If the electric motor flux is constant, the torque of the electric motor is proportional to the current of the q-axis, and the control performance that is similar to that of the DC motor can be obtained. Thus, the control method can be simplified.

III. ELECTRIC MOTOR-PUMP CONTROL STRATEGY RESEARCH

A. ELECTRIC MOTOR-PUMP CONTROL STRATEGY SCHEME

Traditional vector control adopts the PI control method which utilizes the current as the inner loop and the speed as the outer loop. The inner loop is corrected to be a typical I-type system to improve the current response and following ability. In addition, the outer loop is corrected to be a II-type system to enhance the stability of the rotating speed. Based on the previous analysis, PI control characteristics cannot well adapt to the load characteristics of CM. Then, the vector control strategy scheme based on speed sliding mode control shown in Fig. 2 is proposed by adopting SMC-PI to observe the speed.

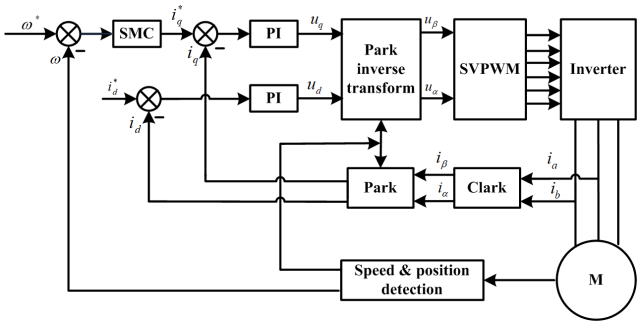

FIGURE 2. Overall scheme of electric motor -pump control strategy.

In the electric motor-pump control system, the disturbance of the current loop is mainly caused by the change in the external counterelectromotive force. Therefore, to ensure the rapid response of the current and make the output torque of the electric motor-pump changing with the load, the current loop adopts the PI control method to meet the requirements of the system.

The system obtains the electric motor-pump speed and rotation position through the resolver, and the target speed and the error of the actual torque are taken as the SMC input. The target value of the q-axis current is obtained through the SMC regulator. The actual values of the AC and DC axes currents are obtained by current sensor sampling and coordinate transformation, and the AC and DC axes voltages are obtained by the PI regulator. Through the Park inverter input vector PWM module, the AC and DC axes voltages can control the switching state of the inverter and realize control of the electric motor-pump.

B. CURRENT REGULATOR DESIGN

In the case of multiple closed-loop control, the design principle of first inner loop and then outer loop is usually used. Therefore, the current regulator is designed first. The current loop mainly includes a current regulator, an inverter, an electric motor and data acquisition, which can be represented by the structure diagram in Fig. 3.

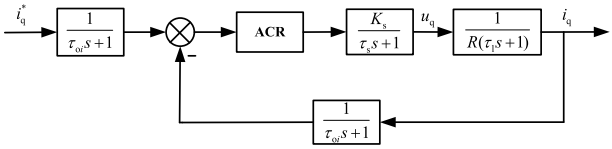

FIGURE 3. Diagram of a current loop.

In Fig. 3, τ_{s}, τ_{oi} and τ_{l} are the time constant of the inverter, the data acquisition system and the delay of the electric motor, respectively. The system satisfies

$$\omega_{\mathrm{ci}} \geq 3\sqrt{\frac{1}{\tau_{\mathrm{oi}}\tau_{\mathrm{s}}}} \tag{13}$$

where ω_{ci} is the cut-off frequency.

Fig. 3 can be further simplified to Fig. 4.

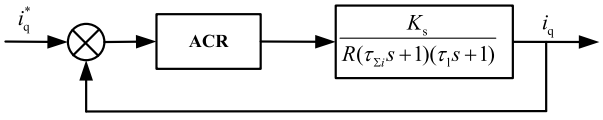

FIGURE 4. Simplified diagram of a current loop.

To correct the current loop to be a typical I-type system, the current regulator can be designed as

$$K_{\mathrm{p}} = \frac{\tau_{\mathrm{s}} s + 1}{\tau_{\mathrm{s}} s} \tag{14}$$

where K_{p} and τ_{s} are the proportional and time constant of the regulator.

Then, the open loop transfer function of the system can be obtained.

$$G(s) = \frac{K_{\mathrm{p}} K_{\mathrm{s}} (\tau_{\mathrm{s}} s + 1)/R}{\tau_{\mathrm{s}} s (\tau_{\Sigma i} s + 1)(\tau_{\mathrm{l}} s + 1)} \tag{15}$$

where, $\tau_{\Sigma i} = \tau_{\mathrm{oi}} + \tau_{\mathrm{s}}$.

Since $\tau_{\Sigma i} \ll \tau_1$, regarding the time constants of the electric motor and the inverter are approximately equal, the transfer function of the system can be obtained.

$$G(s) = \frac{K_p K_s / R}{s(\tau_{\Sigma i} s + 1)} = \frac{\omega_n^2}{s^2 + 2\xi\omega_n s + \omega_n^2} \tag{16}$$

Given $K_I = K_p K_s$, the natural angular frequency and damping of the system can be obtained according to equation (16).

$$\begin{cases} \omega_n = \sqrt{\dfrac{K_I}{\tau_{\Sigma s}}} \\ \zeta = \dfrac{1}{2}\sqrt{\dfrac{1}{K_I \tau_{\Sigma s}}} \end{cases} \tag{17}$$

When $\zeta = 0.707$, it meets the best requirement of the second-order system design.

To satisfy the stability of the system, it should satisfy the following relationship.

$$K_I \tau_{\Sigma s} = 0.5 \tag{18}$$

According to the above requirements, PI parameters of the current controller can be obtained.

$$\begin{cases} K_p = \dfrac{R\tau_1}{2\tau_{\Sigma s} K_s} \\ K_i = \dfrac{K_p}{\tau_1} \end{cases} \tag{19}$$

The theoretical value of PI parameters can be obtained through the above calculation. However, in practical application, the specific value of PI should be adjusted according to the actual control effect.

C. SPEED REGULATOR DESIGN

The speed is adjusted by SMC. According to the control requirements, the input of the adjustment is the difference between the target speed and the actual speed, and the output is q-axis current. In addition, the control structure diagram of the speed SMC regulator can be obtained, as shown in Fig. 5.

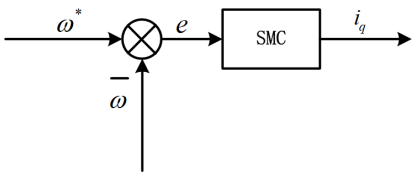

FIGURE 5. SMC regulator diagram of rotating speed.

According to the motion equation of the electric motor,

$$J\frac{d\omega_m}{dt} = \frac{3}{2} p_n \psi_f i_q - T \tag{20}$$

The voltage equation of the electric motor in the two-phase coordinate system, and the two system parameters x_1 and x_2 of sliding mode control defining are defined as,

$$\begin{cases} x_1 = \omega^* - \omega \\ x_2 = \dfrac{dx_1}{dt} = -\omega \end{cases} \tag{21}$$

where ω^* is the target speed of the electric motor, and ω is the actual speed of the electric motor.

The parameters of sliding mode control are substituted into the electric motor motion equation and the voltage equation under the two-phase rotating coordinate system, then equation (21) can be revised as

$$\begin{cases} \dfrac{dx_1}{dt} = \dfrac{T_L}{J} - \dfrac{3P_n \psi_f i_q}{2J} \\ \dfrac{dx_2}{dt} = -\dfrac{3P_n \psi_f i_q'}{2J} \end{cases} \tag{22}$$

Define $u = \frac{di_q}{dt}$ and $D = \frac{3p_n \psi_f}{2J}$. Then, equation (22) can be simplified as

$$\begin{cases} \dfrac{dx_1}{dt} = x_2 - Du \\ \dfrac{dx_2}{dt} = -Du \end{cases} \tag{23}$$

Set the sliding surface function as

$$s = cx_1 + x_2 \tag{24}$$

Take the derivative of equation (24)

$$\frac{ds}{dt} = cx_2 - Du \tag{25}$$

The design purpose of the approach law is to make the moving points rapidly approach the switching surface when they are far away from the switching surface. In addition, the approach law is reduced when the moving points are near the switching surface. Therefore, the speed of control convergence can be improved and the flutter can be reduced. Accordingly, an exponential approach law design is adopted and the controller function is solved as follows

$$u = \frac{1}{D}\left[cx_2 + \varepsilon \mathrm{sgn}(s) + qs\right] \tag{26}$$

where ε is the coefficient of the sign function.

According to equation (24), (25) and (26), the function of the sliding mode controller can be obtained as

$$u(t) = \frac{1}{D}[qce(t) + (c+q)\frac{de(t)}{dt} + \varepsilon \mathrm{sgn}(s)] \tag{27}$$

where $e(t)$ is the speed difference $e(t) = \omega^* - \omega$.

According to equation (27), the relationship between the q-axis current of the electric motor and the speed difference can be obtained as

$$i_q = \frac{1}{D}\int [qce(t) + (c+q)\frac{de(t)}{dt} + \varepsilon \mathrm{sgn}(s)]dt \tag{28}$$

According to equation (28), the function of the sliding mode controller can be obtained. It can be seen from the equation that the q-axis current of the electric motor contains the integral and differential of the speed difference, which can weaken the flutter caused by SMC-PI.

IV. EXPERIMENTAL STUDY

A. TEST PLATFORM BUILDING

To better compare and analyze the performance of the electric motor-pump control strategy, the electric motor-pump loading test platform is built, as shown in Fig. 6. The electric motor-pump control algorithm is completed in the main control circuit and the IGBT module is driven through the drive circuit to control the electric motor-pump. PMSM is used as the loading electric motor and the hydraulic load is simulated by a magnetic powder brake.

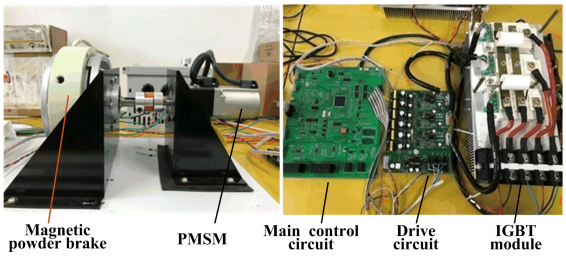

FIGURE 6. Test rig of electric motor loading.

Rated parameters of loading PMSM are shown in TABLE 1

TABLE 1. Parameters of loading electric motor.

Rated power/kW	Rated speed/rpm	Rated current/A	Rated torque/N·m	Pole-pairs
0.1	3000	1.1	950	4

To verify and compare the control performance of PI control and SMC-PI, no-load, load, unload and variable load experiments for the electric motor were carried out. By simulating the changeable characteristics of hydraulic loads, the performance of the electric motor-pump control strategy under different working conditions was analyzed.

B. NO-LOAD TEST

The speed response of the two speed control methods under the no-load condition is shown in Fig. 7. When the target speed was 500 rpm, the rise time of the PI control and SMC-PI was 200 ms and 260 ms, respectively. In addition, the time to steady state was 820 ms and 500 ms, respectively. The speed response time of PI control was slightly faster than that of SMC-PI, but the adjustment time was slightly longer. When using PI control, during the starting period, the electric motor had some overshoot which was approximately 6%. When using SMC-PI, the electric motor speed could basically achieve zero overshoot. Both kinds of speed control realized zero static differential control under the no-load condition.

When the electric motor enters the steady state, the state of u_d and u_q with the vector control strategy based on speed SMC is shown in Fig. 8. Due to the existence of the current adjustment, when the $i_d = 0$ control was adopted, the value of

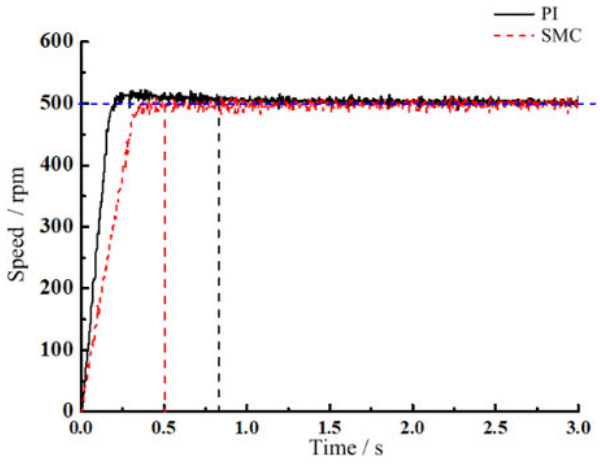

FIGURE 7. SMC/PI speed control response without load.

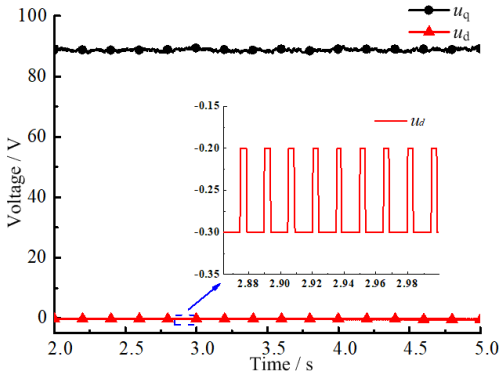

FIGURE 8. Voltage waveform of u_d and u_q.

u_d was basically maintained at approximately zero and there were small oscillations, while u_q maintained stable output.

Changes of u_α and u_β are shown in Fig. 9. In the steady state, they are the standard sine wave, and the amplitude and phase are stable. The results meet the principle of inverse Park transformation.

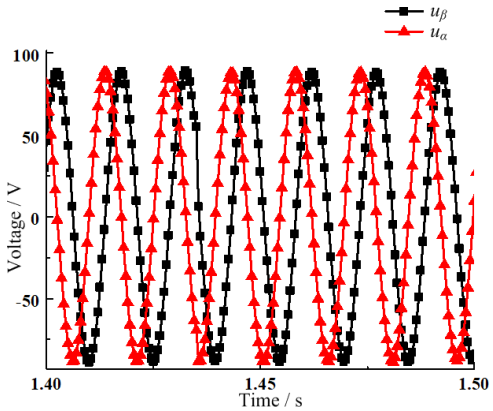

FIGURE 9. Changing process of u_α and u_β.

C. LOADING AND UNLOADING TEST

The speed changes in the two control methods during electric motor loading and unloading conditions are shown in Fig. 10.

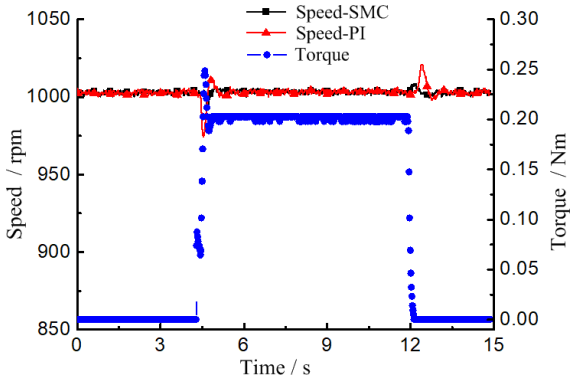

FIGURE 10. Electric motor speed changing under loading and unloading conditions.

The external load was 70% of the rated load of the electric motor. It can be seen from the test results that when PI speed control was adopted, the electric motor speed fluctuated greatly when the load was suddenly loaded and unloaded, and the overshoot was between -2% and 2%. While when SMC-PI was adopted to control the speed, the speed fluctuated only about $-0.7\% \sim 0.5\%$. While the torque had an overshoot of up to 24% when the electric motor was loaded.

The current change in the electric motor controlled by SMC-PI during electric motor loading and unloading conditions is shown in Fig. 11. With the increase in the external load, the current will reach a new balance to increase the output torque. With the decrease in the load, the current will also decrease accordingly. The current loop is controlled by PI. When the load is suddenly increased, the current overshoot is approximately 30%. It can be seen from the local enlarged figure that the phase of the measured current remains stable and the symmetry of the two phases currents is maintained well.

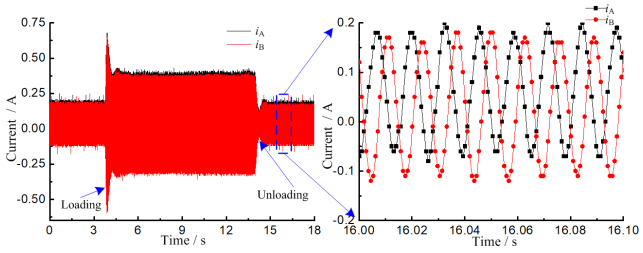

FIGURE 11. Current changing under loading and unloading conditions with SMC-PI.

D. VARIABLE LOAD TEST

Though the electric motor control performance of the two speed control methods under no-load, loading and unloading conditions can be compared, to further analyze the control performance of the two control methods, the variable load is added to the electric motor and tested. The load added to the electric motor under the variable load condition is shown in Fig. 12.

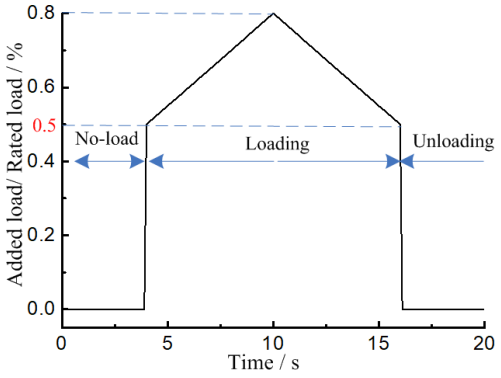

FIGURE 12. The load added under the variable load condition.

The changes in the speed and torque with the PI and SMC-PI under variable load conditions are shown in Fig. 13. It can be seen that during the test process, the electric motor speed fluctuation range is $-2\% \sim 2\%$ with PI control and $-0.5\% \sim 1\%$ with SMC-PI, respectively. The electric motor speed fluctuation range of PI control is $2 \sim 4$ times that of SMC-PI.

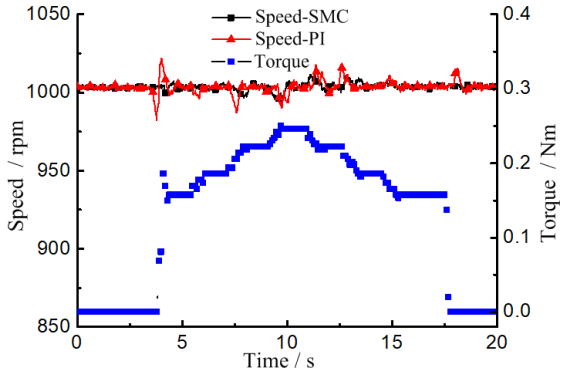

FIGURE 13. Electric motor speed changing with variable load.

TABLE 2 shows the performance comparison of different conditions with different control strategies. It can be seen that SMC-PI can effectively suppress the speed fluctuation, which proves that SMC-PI has better robustness and anti-interference capability and is more suitable for the control requirements of the load characteristics of CM. Though

TABLE 2. Comparison of different control strategies.

Control method	Speed response	Overshoot	Speed fluctuation under loading and unloading conditions	Speed fluctuation under variable load conditions
PI	Faster	2%	-2%-2%	-2%-2%
SMC-PI	Fast	<1%	-0.7%-0.5%	-0.5%-1%

the above tests and comparison, SMC-PI has better speed control performance than PI control under conditions that are similar to hydraulic load characteristics. Though the proposed SMC-PI may introduce flutter and high-order harmonics of the motor into the system due to its switch control, the adopted method of approach law design can suppress the system flutter effectively. In addition, the adaptive method has a certain effect on harmonic reduction.

TABLE 2 shows the performance comparison of loading, unloading and variable load tests with the two control strategies. It can be seen that SMC-PI can effectively suppress the speed fluctuation, which proves that SMC-PI has better robustness and anti-interference capability and is more suitable for the control requirements of CM load characteristics. Through the above tests and comparison under no-load, loading and unloading, and variable load conditions, SMC-PI has better speed control performance than PI control under conditions that are similar to hydraulic load characteristics.

E. ACTUAL CONDITIONS TEST

The load characteristics of the excavator are typical in CM. To further verify the control effects of SMC-PI, relevant tests were carried out on an 8-ton electric excavator prototype. The layout of the test prototype is shown in Fig. 14. It included a lithium battery, a high voltage management unit, a multi-in-one power supply, a vehicle control unit (VCU), an electric motor controller and an electric motor-pump. The instructions of the electric motor controller were sent by VCU and obtained by CAN bus. The rated power of the electric motor was 46.5 kW, the rated current was 91.5 A, and the rated torque was 222 N·m.

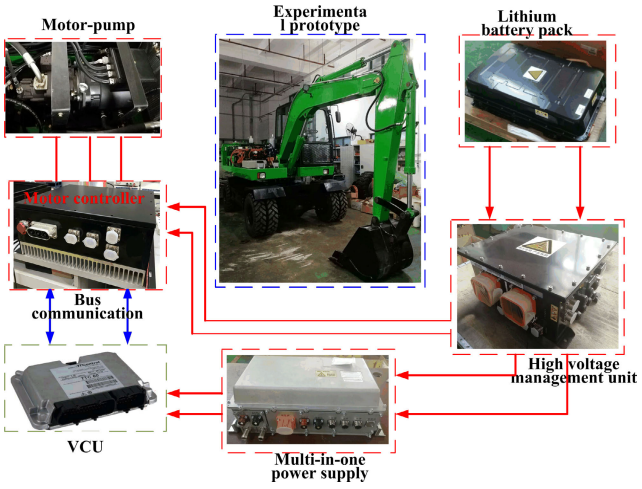

FIGURE 14. Composition of the test prototype.

The proposed vector control algorithm based on SMC-PI control was used to control the main electric motor. The speed curve when the electric motor had no load is shown in Fig. 15. When the target speed was 1,000 rpm, the speed rise time was approximately 350 ms, and there was no overshoot during the speed establishment. In the steady state, the electric motor

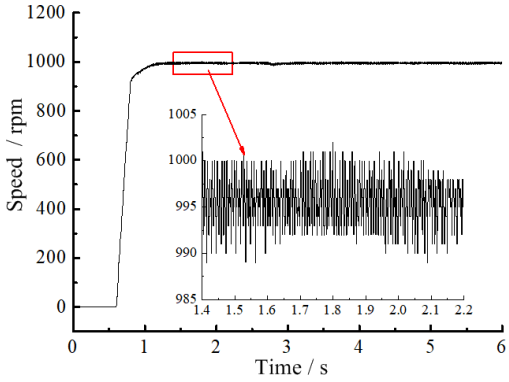

FIGURE 15. Electric motor speed response without load.

speed was adjusted between 990 and 1,000 r/min. In addition, the maximum static difference of the system was approximately 1%.

When the electric motor started with no load, the establishment process of electric motor current is shown in Fig. 16. Seen from the test results, the establishment process of electric motor current was stable during the starting process, and there was no overshoot. The current response time was basically consistent with the speed response time, and the current was approximately 6A in this condition.

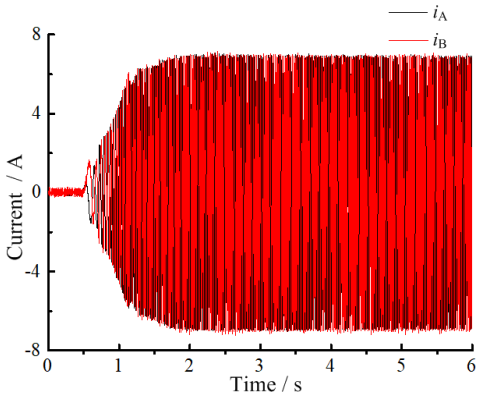

FIGURE 16. Electric motor current response without load.

In the actual operation of a hydraulic excavator, one typical working cycle is basically as follows: boom lifting – composite contraction of arm and bucket - boom descending - excavating - boom lifting - rotating - unloading. The pump outlet pressure of the hydraulic excavator in actual operation is shown in Fig. 17. Pump outlet pressure is periodic and fluctuates violently, and the maximum pressure is nearly 30 MPa. The pump pressure changes with the load according to the actual operation. The speed fluctuates when the load changes suddenly.

When the load power is close to 50% rated power, the electric motor speed fluctuates between $-5\% \sim 5\%$, and the steady-state error is only 0.3%. The adjustment time is short, and the control performance is better.

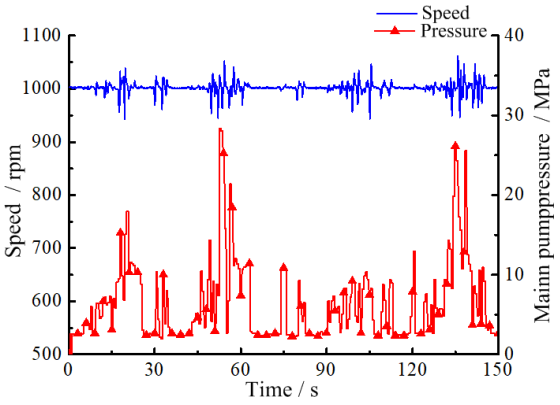

FIGURE 17. Diagram of main pump outlet pressure and speed.

The test results of actual operating conditions show that SMC-PI can be used to adjust the speed to avoid overshooting both speed and current at the starting of the electric motor. When the external load changes dramatically, the electric motor speed fluctuation is small and can be adjusted quickly to maintain the operability of the system.

During the test, the proposed SMC-PI needed complete information about the state of the CM to improve the system control accuracy. Though some progress has been made by using sensorless control or estimating parts of the parameters, the incomplete state information will increase the complexity of system control, and the reliability of the system may be reduced.

V. CONCLUSION

The mathematical model of the hydraulic pump and electric motor was analyzed. According to the load characteristics of CM, the vector control electric motor control strategy was replaced by speed SMC and torque PI control. In addition, it was tested and verified. The main conclusions are as follows:

(1) The electric motor-pump speed overshoot is small, and the static difference is zero when SMC-PI is adopted under no-load, loading, unloading and variable load conditions. When the load changes, the speed fluctuation is approximately 0.5%∼1%, which is only 25%∼50% of PI control.

(2) The maximum static difference of the system is approximately 1% when adopting SMC-PI for the actual operation of the excavator. When the load power is close to 50% rated power, the electric motor-pump speed fluctuates between -5%∼5%, and the steady-state error is only 0.3%. The adjustment time is short, and the control performance is better.

(3) SMC-PI has better robustness and anti-interference capability and is more suitable for CM which has complicated and changeable loads.

The proposed SMC-PI control, which has excellent robustness, can ensure a better motor control performance of CM than other control methods. The working conditions of pure electric CM are complex and changeable. The control algorithm of the motor controller can be developed according to the positive/negative flow rate, load sensing and other different systems to match the system requirements for flow rate and torque. Then, different control methods can be chosen according to the CM working conditions to achieve the requirements of high efficiency or energy-saving of the motor. Therefore, the energy consumption and operating cost of the whole machine can be reduced.

REFERENCES

[1] T. Wang and Q. Wang, "Control system of permanent magnet generator for boom potential energy recovery," *Trans. Chin. Soc. Agricult. Mach.*, vol. 45, no. 11, pp. 34–39, 2014.

[2] Q. Chen, T. Lin, and H. Ren, "Direct torque control of a permanent magnet synchronous machine for hybrid hydraulic excavator," *IET Electr. Power Appl.*, vol. 13, no. 2, pp. 222–228, Feb. 2019.

[3] S. Hang, H. Yao, and Y. Wei, "Design of electric driving swing system in hybrid excavator," *Electr. Driv.*, vol. 48, no. 3, pp. 47–50, 2018.

[4] J. LIN, Q. Tu, and S. Zou, "MTPA flexible control based on the torque limit of the IPMSM vector control system," *Electr. Drives*, vol. 47, no. 1, pp. 55–58, 2017.

[5] X.-H. Chang and G.-H. Yang, "Nonfragile H_∞ filter design for T–S fuzzy systems in standard form," *IEEE Trans. Ind. Electron.*, vol. 61, no. 7, pp. 3448–3458, Jul. 2014.

[6] J. Yao and W. Deng, "Active disturbance rejection adaptive control of uncertain nonlinear systems: Theory and application," *Nonlinear Dyn.*, vol. 89, no. 3, pp. 1611–1624, Aug. 2017.

[7] X. Zhang and G. H. B. Foo, "A constant switching frequency-based direct torque control method for interior permanent-magnet synchronous motor drives," *IEEE/ASME Trans. Mechatronics*, vol. 21, no. 3, pp. 1445–1456, Jun. 2016.

[8] J. Holtz, "Sensorless control of induction machines—With or without signal injection?" *IEEE Trans. Ind. Electron.*, vol. 53, no. 1, pp. 7–30, Feb. 2006.

[9] H. Zhang, A. Hu, and J. Li, "Fuzzy PI speed control of brushless DC motor," *J. Kuming Univ. Sci. Technol.*, vol. 32, no. 2, pp. 52–55, 2007.

[10] J. Zhao and H. Zhang, "Parameter optimization of PID controller for AC speed regulating system based on adaptive genetic algorithm," *Micromotors*, vol. 41, no. 1, pp. 34–36, 2008.

[11] L. Wen, M. Yang, X. He, L. Luo, and W. Chen, "Application of fuzzy PID control based on AGA in experimental rolling MIL," *Mach. Tool Hydraul.*, vol. 39, no. 17, pp. 26–29, 2011.

[12] X. Wang and Z. Xu, "Speed regulation control of switched reluctance motors based on PI parameter self-adaptation," *Proc. CSEE*, vol. 35, no. 16, pp. 4215–4223, 2015.

[13] A. Roy and S. Srivastava, "Design of optimal PIλDδ controller for speed control of DC motor using constrained particle swarm optimization," in *Proc. Int. Conf. Circuit Power Comput. Technol.*, Mar. 2016, pp. 1–6.

[14] H. Tayara, D. J. Lee, and K. T. Chong, "Auto PID tuning of speed control of DC motor using particle swarm optimization based on FPGA," *Appl. Mech. Mater.*, vol. 776, pp. 390–395, Jul. 2015.

[15] H. Wang and S. Kang, "Adaptive neural command filtered tracking control for flexible robotic manipulator with input dead-zone," *IEEE Access*, vol. 7, pp. 22675–22683, 2019.

[16] H. Wang, P. X. Liu, J. Bao, X.-J. Xie, and S. Li, "Adaptive neural output-feedback decentralized control for large-scale nonlinear systems with stochastic disturbances," *IEEE Trans. Neural Netw. Learn. Syst.*, vol. 31, no. 3, pp. 972–983, Mar. 2020.

[17] M. Tursini, R. Petrella, and F. Parasiliti, "Adaptive sliding-mode observer for speed-sensorless control of induction motors," *IEEE Trans. Ind. Appl.*, vol. 36, no. 5, pp. 1380–1387, Sep./Oct. 2000.

[18] Y. Jiang, W. Xu, C. Mu, and Y. Liu, "Improved deadbeat predictive current control combined sliding mode strategy for PMSM drive system," *IEEE Trans. Veh. Technol.*, vol. 67, no. 1, pp. 251–263, Jan. 2018.

[19] W. K. Wibowo and S.-K. Jeong, "Improved estimation of rotor position for sensorless control of a PMSM based on a sliding mode observer," *J. Central South Univ.*, vol. 23, no. 7, pp. 1643–1656, Jul. 2016.

[20] S. Y. Chen, Y. G. Pi, "Research on PMSM control for position sensorless based on fractional PD sliding mode observer," *Appl. Mech. Mater.*, vols. 494–495, pp. 1028–1035, Feb. 2014.

[21] Y. Wang, H. R. Karimi, H. Shen, Z. Fang, and M. Liu, "Fuzzy-model-based sliding mode control of nonlinear descriptor systems," *IEEE Trans. Cybern.*, vol. 49, no. 9, pp. 3409–3419, Sep. 2019.
[22] Y. Wang, B. Jiang, Z.-G. Wu, S. Xie, and Y. Peng, "Adaptive sliding mode fault-tolerant fuzzy tracking control with application to unmanned marine vehicles," *IEEE Trans. Syst., Man, Cybern. Syst.*, early access, Jan. 24, 2020, doi: 10.1109/TSMC.2020.2964808.
[23] W. Wei, "Research on PMSM AC servo system based on sliding mode control," M.S. thesis, Dept. Electron. Eng., Beijing Jiaotong Univ., Beijing, China, 2018.
[24] H.-T. Moon, H.-S. Kim, and M.-J. Youn, "A discrete-time predictive current control for PMSM," *IEEE Trans. Power Electron.*, vol. 18, no. 1, pp. 464–472, Jan. 2003.
[25] F. Morel, X. Lin-Shi, J.-M. Retif, B. Allard, and C. Buttay, "A comparative study of predictive current control schemes for a permanent-magnet synchronous machine drive," *IEEE Trans. Ind. Electron.*, vol. 56, no. 7, pp. 2715–2728, Jul. 2009.
[26] A. A. Ahmed, J.-S. Kim, and Y. I. Lee, "Model predictive torque control of PMSM for EV drives: A comparative study of finite control set and predictive dead-beat control schemes," in *Proc. 18th Int. Middle East Power Syst. Conf. (MEPCON)*, Dec. 2016, pp. 156–163.

SHENGJIE FU received the Ph.D. degree in information science and engineering from Xiamen University. He joined the College of Mechanical Engineering and Automation, Huaqiao University, in 2012. His research interests include energy saving technology of electro hydraulic transmission and design of advanced equipment.

HAOLING REN received the M.S. degree in mechatronic engineering from the Harbin Institute of Technology, in 2003, and the Ph.D. degree in mechatronic engineering from the State Key Laboratory of Fluid Power and Mechatronic Systems, Zhejiang University, in 2014. She is currently an Associate Director of the Department of Mechatronic, College of Mechanical Engineering and Automation, Huaqiao University. Her research interest includes energy saving technology of electro hydraulic transmission.

TIANLIANG LIN received the Ph.D. degree in mechatronic engineering from the State Key Laboratory of Fluid Power and Mechatronic Systems, Zhejiang University. He joined the College of Mechanical Engineering and Automation, Huaqiao University, in 2016. He is currently an Associate Professor and the Director of the Department of Mechatronic. His research interests include energy saving technology of electro hydraulic transmission and design of advanced equipment.

SHENGYAN ZHOU is currently pursuing the master's degree with Huaqiao University. His research interests include induction electro-hydraulic transmission and control and power system energy saving technology.

QIHUAI CHEN (Member, IEEE) received the Ph.D. degree in mechatronic engineering from the State Key Laboratory of Fluid Power and Mechatronic Systems, Zhejiang University. He joined the College of Mechanical Engineering and Automation, Huaqiao University, in 2016, which works with team partner to study on construction machinery energy conservation technology. His research interests include design and control of permanent magnet machines in hybrid power systems and electric power systems.

ZHONGSHEN LI received the Ph.D. degree in mechatronic engineering from Huaqiao University. He is currently a Professor with Huaqiao University. His research interests include industrial automation control and advanced control algorithm.